Global Control of Suprathreshold Reactivity by Quantized Transition States

ARTICLE *in* JOURNAL OF THE AMERICAN CHEMICAL SOCIETY · JANUARY 1991

Impact Factor: 12.11 · DOI: 10.1021/ja00002a016

$(CD_3)_3CH$ supported the greater reactivity of the tertiary vs primary C–H bonds in isobutane toward initial oxidative insertion by the metal center.

The above results lead us to conclude that the relative reactivities of C–H bonds of alkanes in oxidative insertion reactions with $(OC)_3Mn^-$ and $(OC)_2Fe^-$ is *tertiary* ≥ *secondary* > *primary*. This extends the C–H bond relative reactivity scale reported in the condensed phase to include tertiary C–H bonds.[5,6] The apparent absence of oxidative insertion into tertiary C–H bonds in the condensed-phase studies was attributed to steric effects with the $(\eta^5\text{-}C_5Me_5)ML_2$ complexes.[5] While we cannot discount steric effects in the present gas-phase negative ions, the steric effects in reactions with $(OC)_3Mn^-$ and $(OC)_2Fe^-$ should be considerably smaller than those experienced with the condensed-phase complexes containing the bulky $\eta^5\text{-}C_5(CH_3)_5$ ligand. However, such considerations must await structural information for the two MCMEU transition-metal complex negative ions.[40,41]

Acknowledgment. We gratefully acknowledge support for this research from the National Science Foundation and discussions of the isotope effects with Professors D. W. Setser and R. L. Schowen.

(40) Poliakoff and Turner (Poliakoff, M.; Turner, *J. Chem. Soc., Dalton Trans.* **1973**, 1351; **1974**, 2276. Poliakoff, M. *Ibid.* **1974**, 210) determined the structure of $Fe(CO)_3$, which is isoelectronic with $(OC)_3Mn^-$, in low-temperature matrices to be of C_{3v} symmetry with the OC–Fe–CO angle ~110°, slightly distorted from a planar structure.

(41) Guenzburger et al. (Guenzgurger, D.; Saitovitch, E. M. B.; De Paoli, M. A.; Manela, H. *J. Chem. Phys.* **1984**, *80*, 735) reported molecular orbital studies on $Fe(CO)_5$ and its photofragments $Fe(CO)_n$ where n = 1–4. The linear and a bent geometry for $Fe(CO)_2$ were examined.

Global Control of Suprathreshold Reactivity by Quantized Transition States

David C. Chatfield,[†] Ronald S. Friedman,[†] Donald G. Truhlar,*[,†] Bruce C. Garrett,[‡] and David W. Schwenke[§]

Contribution from the Department of Chemistry and Supercomputer Institute, University of Minnesota, Minneapolis, Minnesota 55455-0431, the Molecular Science Research Center, Pacific Northwest Laboratory, Richland, Washington 99352, and the NASA Ames Research Center, Moffett Field, California 94035. *Received April 20, 1990. Revised Manuscript Received August 14, 1990*

Abstract: We present evidence that the accurate quantum mechanical probability of the reaction of H with H_2 is globally controlled by quantized transition states up to very high energies. The quantized transition states produce steplike features in the cumulative reaction probability curves that are analyzed up to energies of 1.6 eV; the analysis clearly associates these steps (or "thresholds") with quantized dynamical bottlenecks that control the passage of reactive flux to products. We have assigned bend and stretch quantum numbers to the modes orthogonal to the reaction coordinate for all these transition states on the basis of threshold energies of semiclassical vibrationally adiabatic potential energy curves and vibrationally specific cumulative reaction probability densities.

1. Introduction

A subject that has received increasing attention over the past several years is the role of transition states[1,2] and phase space structures[3] as dynamical bottlenecks to flux flow in classical mechanics. Some progress is also being made in understanding the relevance of these results to quantum dynamics,[4] and variational and other generalized transition-state theory calculations based on quantized transition states[2,5-7] have proved very successful in reproducing accurate quantum dynamical rate constants. As a result we have gained considerable confidence in the dominance of threshold behavior of chemical reactivity by vibrationally adiabatic dynamical bottlenecks,[5,6,8] and these have been shown to exert control not only at un-state-selected reaction thresholds but also at thresholds for some vibrationally excited reactions.[5a,5h,9] In the present paper we present numerical evidence that quantized dynamical bottlenecks limit the accurate quantum dynamical flux from reactants to products in a chemical reaction in a much more global way.

We have studied the energy dependence of the cumulative reaction probability[10] (hereafter referred to as the CRP) for the H + H_2 reaction for various values of the total angular momentum J. The quantum mechanical CRP, which we denote $N^J_{\alpha\alpha'}(E)$, is defined as the sum over all state-to-state ($n \rightarrow n'$) reactive transition probabilities $P^J_{\alpha n\alpha' n'}(E)$ from a given initial chemical arrangement α to a final chemical arrangement α'

$$N^J_{\alpha\alpha'}(E) = \sum_n \sum_{n'} P^J_{\alpha n\alpha' n'}(E) \quad (1)$$

where n denotes the collection of all initial quantum numbers and n' denotes the set of final ones. For example, for an atom–diatom

[†] University of Minnesota.
[‡] Pacific Northwest Laboratory.
[§] NASA Ames Research Center.

(1) (a) Keck, J. C. *Adv. Chem. Phys.* **1967**, *13*, 85. (b) Pechukas, P.; McLafferty, F. J. *J. Chem. Phys.* **1973**, *58*, 1622. (c) Pollak, E.; Pechukas, P. *J. Chem. Phys.* **1978**, *69*, 1218. (d) Garrett, B. C.; Truhlar, D. G. *J. Phys. Chem.* **1979**, *83*, 1052. (e) Garrett, B. C.; Truhlar, D. G. *J. Phys. Chem.* **1980**, *84*, 805. (f) Chesnavich, W. J.; Su, T.; Bowers, M. In *Kinetics of Ion Molecule Reactions*; Ausloos, P., Ed.; Plenum: New York, 1979; p 31. (g) Chesnavich, W. J.; Bass, L.; Su, T.; Bowers, M. J. *J. Chem. Phys.* **1981**, *74*, 2228. (h) Doll, J. D. *J. Chem. Phys.* **1981**, *74*, 1074.

(2) For a review see: Truhlar, D. G.; Hase, W. L.; Hynes, J. T. *J. Phys. Chem.* **1983**, *87*, 2664, 5523E.

(3) (a) Davis, M. J. *J. Chem. Phys.* **1987**, *86*, 3978. (b) Skodje, R. T.; Davis, M. J. *J. Chem. Phys.* **1988**, *88*, 2429. (c) DeLeon, N.; Mehta, M. A.; Topper, R. Q. Unpublished results.

(4) See, for example: Marcus, R. A. *Ber. Bunsenges. Phys. Chem.* **1977**, *81*, 190. Marston, C. C.; Wyatt, R. E. *ACS Symp. Ser.* **1984**, *No. 263*, 441. Brown, R. C.; Wyatt, R. E. *Phys. Rev. Lett.* **1986**, *57*, 1. Skodje, R. T.; Rohrs, H. W.; VanBuskirk, J. *Phys. Rev. A* **1989**, *40*, 2894, and references cited therein. See also: Gomez Llorente, J. M.; Hahn, O.; Taylor, H. S. *J. Chem. Phys.* **1990**, *92*, 2762.

(5) (a) Garrett, B. C.; Truhlar, D. G. *J. Phys. Chem.* **1979**, *83*, 1079. (b) Truhlar, D. G.; Garrett, B. C. *Acc. Chem. Res.* **1980**, *13*, 440. (c) Truhlar, D. G.; Isaacson, A. D.; Skodje, R. T.; Garrett, B. C. *J. Phys. Chem.* **1982**, *86*, 2252. (d) Rai, S. N.; Truhlar, D. G. *J. Chem. Phys.* **1983**, *79*, 6046. (e) Truhlar, D. G.; Garrett, B. C. *Annu. Rev. Phys. Chem.* **1984**, *35*, 159. (f) Isaacson, A. D.; Sund, M. T.; Rai, S. N.; Truhlar, D. G. *J. Chem. Phys.* **1985**, *82*, 1338. (g) Garrett, B. C.; Truhlar, D. G.; Schatz, G. C. *J. Am. Chem. Soc.* **1986**, *108*, 2876. (h) Garrett, B. C.; Truhlar, D. G.; Varandas, A. J. C.; Blais, N. C. *Int. J. Chem. Kinet.* **1986**, *18*, 1065. (i) Truhlar, D. G.; Garrett, B. C. *J. Chim. Phys.* **1987**, *84*, 365.

0002-7863/91/1513-486$02.50/0

reaction, A + BC → AB + C, $n(n')$ denotes the collection of the initial (final) vibrational quantum number $v(v')$, rotational quantum number $j(j')$, and orbital angular momentum quantum number $l(l')$. The CRP is a unitless function that contains all the dynamical information needed to calculate an ordinary (as in rate = k[A][BC]) temperature-dependent rate coefficient $k(T)$. In particular, the rate coefficient for a canonical ensemble at temperature T may be written[11]

$$k(T) = \frac{\sum_J (2J+1) \int_0^\infty dE \exp(-E/\tilde{k}T) \phi^{R,J}(E) k^J(E)}{\Phi^R(T)} \quad (2)$$

where $\tilde{k}$ is Boltzmann's constant, $\Phi^R(T)$ is the reactants' partition function per unit volume at temperature T, $\phi^{R,J}(E)$ is the reactants' density of states (with total angular momentum J) per unit energy per unit volume, and $k^J(E)$ is the rate coefficient for a microcanonical ensemble of binary collisions with total angular momentum J and total energy E. The microcanonical rate coefficient is

$$k^J(E) = N^J_{\alpha\alpha'}(E)/h\phi^{R,J}(E) \quad (3)$$

Thus, we should think of the CRP as a unitless version of the microcanonical rate coefficient.

We will center our attention on the energy derivative of the CRP, i.e.

$$\rho^J_{\alpha\alpha'}(E) = dN^J_{\alpha\alpha'}/dE \quad (4)$$

This will be called the density of reactive states, and we will show that $\rho^J_{\alpha\alpha'}$ as a function of E may be interpreted as a reactivity spectrum of generalized transition states.

The present calculations were carried out for the reaction H + H'H'' → HH' + H'', where H, H', and H'' are hydrogen atoms, treated as distinguishable. The overall distinguishable atom reaction probability may be obtained by multiplying by a factor of 2 to account for the two symmetry-related reaction paths. The actual observable reaction rate (i.e., the para-ortho conversion rate) may be obtained within about 1%[12] from the distinguishable atom rates by multiplying by $^3/_4$, a factor that arises from simple spin considerations,[13] so the effects of particle indistinguishability need not be considered explicitly here.

Previous work on the H + H_2 reaction has been quite extensive,[14] and we summarize here only a few of the previous observations that are especially relevant to our new work presented below. The reaction threshold for H + H_2 has been found to be well predicted by a vibrationally adiabatic model,[12,15] and the canonical ensemble rate constants are well predicted by variational transition-state theory with multidimensional tunneling corrections.[5g,16] The rate coefficient of this theory involves a generalized transition-state theory partition function obtained by summing over the quantized energy levels of an intermediate configuration with one degree of freedom missing,[5,6] as in conventional[17] transition-state theory. The rate constants are also well predicted by a reduced-dimensionality theory involving sums over reaction probabilities associated with various bend-excited states of an H_3 generalized transition state.[7b,18] For the most part the dynamics are "direct", i.e., there are no trapped states, but at selected energies, the state-to-state reaction probabilities show oscillations which may be associated with short-lived metastable quasibound states.[19] The most complete analyses of the H_3 metastable states reported to date are those of Cuccaro et al.[20] and of the present authors and co-workers.[21] In a beautiful study, Cuccaro et al.[20] have assigned quantum numbers to 8 J = 0 and 14 J = 1 metastable states in the energy interval from threshold up to 1.7 eV.

One difficulty with analyzing the oscillations in detail is that, as first pointed out[22] in studies of reduced-dimensionality reactive systems, H_3 metastable states are not well described by the standard[23] multichannel isolated, narrow resonance formulas. If these formulas held, one could completely characterize the metastable states by channel-independent complex energies and partial widths. Instead, however, it was found that the values of these parameters depend significantly on which state-to-state reaction probabilities and scattering matrix elements are analyzed.[21,22] One possible way to achieve a channel-independent characterization of the resonances would be to analyze their effect on the CRP defined above. With this as one motivation we calculated accurate quantum mechanical CRPs as functions of energy for various J. The results, which are presented in this paper, are very well converged, so we were able to perform stable numerical differentiation to calculate the density of reactive states defined by eq 4. As we will see below, the structure of $N^J_{\alpha\alpha'}(E)$ and $\rho^J_{\alpha\alpha'}(E)$ is amazingly well explained by a series of quantized thresholds. At this point we make a critical conceptual distinction between two kinds of states of H_3. Trapped states are quasibound (typically short-lived) states with a full set of linear triatomic quantum numbers[19,24] ($v_1v_2^Kv_3$), which—just as for, say, CO_2—correspond to symmetric stretch (v_1), bend (v_2), vibrational angular momentum (K), and asymmetric stretch (v_3). The other kind of

(6) Truhlar, D. G.; Isaacson, A.; Garrett, B. C. In *Theory of Chemical Reaction Dynamics*; Baer, M., Ed.; CRC Press: Boca Raton, FL, 1985; Vol. 4, p 65.

(7) (a) Bowman, J. M. *Adv. Chem. Phys.* **1985**, *61*, 115. (b) Bowman, J. M.; Wagner, A. F. In *The Theory of Chemical Reaction Dynamics*; Clary, D. C., Ed.; Reidel: Dordrecht, 1986; p 47.

(8) (a) Eliason, M. A.; Hirschfelder, J. O. *J. Chem. Phys.* **1959**, *30*, 1426. (b) Marcus, R. A. *J. Chem. Phys.* **1967**, *46*, 959. (c) Marcus, R. A. *Discuss. Faraday Soc.* **1967**, *44*, 7. (d) Child, M. S. *Discuss. Faraday Soc.* **1967**, *44*, 68. (e) Truhlar, D. G. *J. Chem. Phys.* **1970**, *53*, 2041. (f) Bowman, J. M.; Kuppermann, A.; Adams, J. T.; Truhlar, D. G. *Chem. Phys. Lett.* **1973**, *20*, 229. (g) Duff, J. W.; Truhlar, D. G. *Chem. Phys. Lett.* **1973**, *23*, 327.

(9) (a) Truhlar, D. G.; Isaacson, A. D. *J. Chem. Phys.* **1982**, *77*, 3516. (b) Pollak, E.; Wyatt, R. E. *J. Chem. Phys.* **1983**, *78*, 4464. (c) Steckler, R.; Truhlar, D. G.; Garrett, B. C.; Blais, N. C.; Walker, R. B. *J. Chem. Phys.* **1984**, *81*, 5700. (d) Garrett, B. C.; Truhlar, D. G. *J. Phys. Chem.* **1985**, *89*, 2204. (e) Garrett, B. C.; Truhlar, D. G. *Int. J. Quantum Chem.* **1986**, *29*, 1463. (f) Garrett, B. C.; Truhlar, D. G.; Bowman, J. M.; Wagner, A. F. *J. Phys. Chem.* **1986**, *90*, 4305. (g) Haug, K.; Schwenke, D. W.; Shima, Y.; Truhlar, D. G.; Zhang, J.; Kouri, D. J. *J. Phys. Chem.* **1986**, *90*, 6757. (h) Haug, K.; Schwenke, D. W.; Truhlar, D. G.; Zhang, Y.; Zhang, J. Z. H.; Kouri, D. J. *J. Chem. Phys.* **1987**, *87*, 1892. (i) Zhang, J. Z. H.; Zhang, Y.; Kouri, D. J.; Garrett, B. C.; Haug, K.; Schwenke, D. W.; Truhlar, D. G. *Faraday Discuss. Chem. Soc.* **1987**, *84*, 371.

(10) The useful terminology "cumulative reaction probability" was apparently coined in: Miller, W. H. *J. Chem. Phys.* **1975**, *62*, 1899. See also: Miller, W. H. In *Potential Energy Surfaces and Dynamics Calculations*; Truhlar, D. G., Ed.; Plenum: New York, 1981; p 265.

(11) Equations 1–3 are equivalent to eq 233 of ref 6. See also refs 1d, 7a, 8a, 9, and: (a) Eyring, H.; Walter, J.; Kimball, G. E. *Quantum Chemistry*; Wiley: New York, 1944. (b) Kuppermann, A. *J. Phys. Chem.* **1979**, *83*, 171. (c) Christov, S. G. *Collision Theory and Statistical Theory of Chemical Reactions*; Springer-Verlag: Berlin, 1980.

(12) Schatz, G. C.; Kuppermann, A. *J. Chem. Phys.* **1976**, *65*, 4668.

(13) Truhlar, D. G. *J. Chem. Phys.* **1976**, *65*, 1008.

(14) For reviews see: (a) Truhlar, D. G.; Wyatt, R. E. *Annu. Rev. Phys. Chem.* **1976**, *27*, 1. (b) Valentini, J. J.; Phillips, D. L. In *Bimolecular Collisions*; Ashfold, M. N. R., Baggott, J. E., Eds.; Royal Society of Chemistry: London, 1989; p 1.

(15) Marcus, R. A. *J. Chem. Phys.* **1964**, *41*, 610. Truhlar, D. G.; Kuppermann, A. *J. Chem. Phys.* **1972**, *56*, 2232.

(16) (a) Garrett, B. C.; Truhlar, D. G. *Proc. Natl. Acad. Sci. U.S.A.* **1979**, *76*, 4755. (b) Garrett, B. C.; Truhlar, D. G.; Grev, R. S.; Magnuson, A. W. *J. Phys. Chem.* **1980**, *84*, 1730.

(17) (a) Wigner, E. *Z. Phys. Chem.* **1932**, *B15*, 203. (b) Eyring, H. *J. Chem. Phys.* **1935**, *3*, 107. (c) Evans, M. G.; Polanyi, M. *Trans. Faraday Soc.* **1935**, *31*, 875.

(18) See also: Sun, Q.; Bowman, J. M. *J. Phys. Chem.* **1990**, *94*, 718, for similar treatments of the D + H_2 and H + D_2 reactions.

(19) For reviews (and some new work) of quasibound states in reactive collisions, with special attention to H_3, see: (a) Kuppermann, A. In *Potential Energy Surfaces and Dynamics Calculations*; Truhlar, D. G., Ed.; Plenum: New York, 1981; p 375. (b) Garrett, B. C.; Schwenke, D. W.; Skodje, R. T.; Thirumalai, D.; Thompson, T. C.; Truhlar, D. G. *ACS Symp. Ser.* **1984**, *No. 263*, 375.

(20) Cuccaro, S. A.; Hipes, P. G.; Kuppermann, A. *Chem. Phys. Lett.* **1989**, *157*, 440.

(21) Zhao, M.; Mladenovic, M.; Truhlar, D. G.; Schwenke, D. W.; Sharafeddin, O.; Sun, Y.; Kouri, D. J. *J. Chem. Phys.* **1989**, *91*, 5302.

(22) Schwenke, D. W.; Truhlar, D. G. *J. Chem. Phys.* **1987**, *87*, 1095.

(23) Taylor, J. R. *Scattering Theory*; Wiley: New York, 1972.

(24) The notation is standard: Herzberg, G. *Molecular Spectra and Molecular Structure. II. Infrared and Raman Spectra of Polyatomic Molecules*; van Nostrand: Princeton, 1945; except we use K instead of l because l is reserved for orbital angular momentum in collision theory.

state discussed in this paper is a "quantized transition state", also called a "threshold" or a "quantized dynamical bottleneck". This kind of state, since it is a generalized transition state,[5,9,16b] is missing one degree of freedom,[17] the reaction coordinate, and so it has only the $(v_1v_2^K)$ quantum numbers. In addition, since the dynamical bottlenecks need not have $D_{\infty h}$ symmetry (the H–H′ bond may be longer than the H′–H″ bond), the vibration transverse to the reaction coordinate need not be symmetric, and so v_1 will be called the stretch quantum number rather than the symmetric stretch. Both trapped states and thresholds are associated with time delays (trapped states because their dissociative motion is reflected and thresholds because the local velocity along the reaction coordinate approaches zero at a threshold). The effects of trapped states have been widely discussed.[19] In the present paper we show that although the effect of trapped states may be very important in state-to-state cross sections, the effect of thresholds is much more pronounced in overall rate coefficients. Although our examples in this paper are all based on the prototype H + H_2 reaction, we expect that the conclusions are more general.[25]

Before closing this introduction, we mention one further motivation for the present study. Although accurate CRPs for H + H_2 have *not* been published previously, our group did publish an accurate CRP for the O + H_2 reaction,[9h,9i] and we used it to explain why variational transition-state theory with formally adiabatic ground-state transmission coefficients predicts accurate thermal rate constants even for reactions that are rotationally nonadiabatic. Then, in a very stimulating followup study, Bowman[26] discussed the structure in our accurate quantum CRP in terms of bend-excited transition states. This helps motivate the search for similar structures in the H + H_2 CRP and their more quantitative analysis and interpretation.

2. Calculations

Converged quantum dynamics calculations were carried out by using a double-many-body expansion (DMBE)[27] of the potential energy surface. The high accuracy of this energy surface has recently been verified by new state-of-the-art electronic structure calculations.[28] Since the potential energy surface is very accurate and the quantum dynamics calculations are converged, the CRPs analyzed here represent accurate microcanonical rate constants for a real chemical reaction, which makes our conclusions more interesting than if we had carried out model studies.

We have performed calculations for many combinations of total angular momentum and total energy, including fine-grid energy scans for $J = 0$, 1, and 4. The most noticeable effects of overall rotation are a shift in energy of the quantized transition states (see below) by about $BJ(J + 1)$, where B is a rotational constant[7,19b,21,24] of H_3, and an increased density of states due to nonzero components of vibrational angular momentum becoming allowed. (Note that $K \leq J$ and $K = v_2, v_2 - 2, v_2 - 4, \ldots, 0$ or 1. The degeneracy of a state is $2 - \delta_{K0}$.)

The quantum dynamics calculations were carried out by the generalized Newton variational principle for the amplitude density, as described previously.[29] We refer the reader to other papers[21,30] for details of the basis sets, numerical parameters, and convergence checks. We carried out calculations for $J = 0$ at 258 energies in the range 0.27–1.66 eV. Convergence tests using a different parameter set indicate that error in the cumulative reaction probability is less than 0.1% for energies up to 1.2 eV and less than 0.6% for energies up to 1.66 eV, the highest energy studied. We also carried out converged quantum dynamics calculations for $J = 1$ at 118 energies and for $J = 4$ at 97 energies in the range 0.30–1.66 eV.

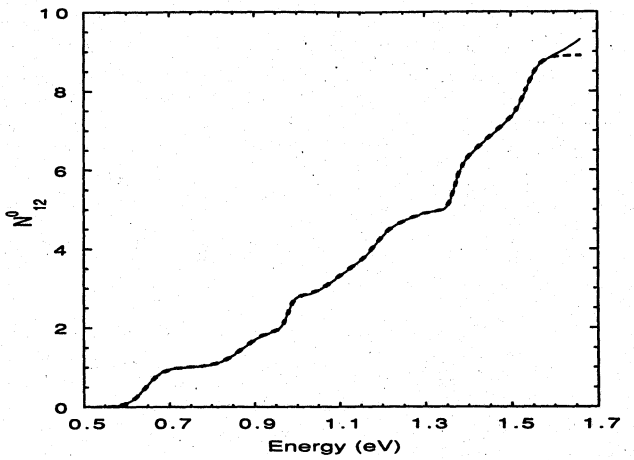

Figure 1. Cumulative reaction probability for $J = 0$. The solid curve is a spline fit to the accurate quantal results, and the dashed curve is obtained by integrating the synthetic density curve shown in Figure 2.

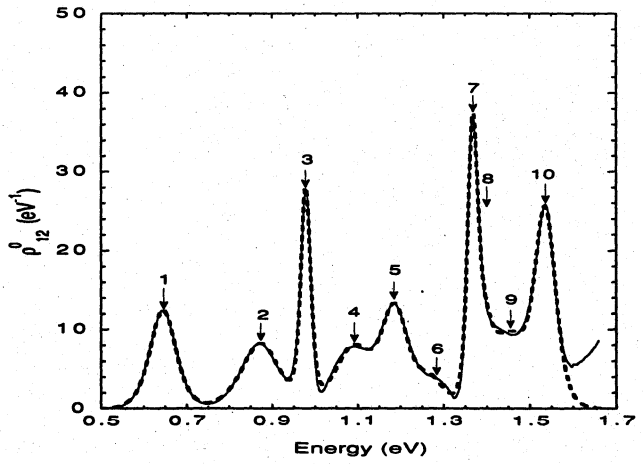

Figure 2. Density of reactive states for $J = 0$. The solid curve is obtained by differentiating the solid curve in Figure 1, and the dashed curve is the second fit discussed below eq 10. The feature numbers in this figure and Figure 5 are positioned at the V_β values from this second fit.

3. Interpretation

$J = 0$. Figure 1 shows the accurate quantal $N^J_{\alpha\alpha'}(E)$ vs E for $J = 0$ as a solid curve; it shows that the cumulative reaction probability as a function of energy is characterized by steplike structures. The derivative of the cumulative reaction probability with respect to energy was calculated by analytically differentiating the cubic spline fit shown as the solid curve in Figure 1. The resulting density function for $J = 0$ is plotted as a solid curve in Figure 2, and in this curve we see resolved structural features at energies up to higher than 1.5 eV. This treatment of the data clearly reveals a spectrum of discrete thresholds underlying the CRP. A zero-order interpretation immediately is suggested by the fact that the CRP in Figure 1 reaches 9 at the upper end of the energy range, and there are seven peaks and two discernible shoulders in Figure 2. Each peak or shoulder may be intrepreted as a quantized transition state admitting one unit of overall re-

(25) A special case where trapped states may have a more significant effect on rate coefficients is when they occur below the overall quasiclassical reaction threshold. So far, examples of this effect are known only for model problems: Child, M. S. *Mol. Phys.* **1967**, *12*, 401. Garrett, B. C.; Truhlar, D. G.; Grev, R. S.; Schatz, G. C.; Walker, R. B. *J. Phys. Chem.* **1981**, *85*, 3806.

(26) Bowman, J. M. *Chem. Phys. Lett.* **1987**, *141*, 545.

(27) Varandas, A. J. C.; Brown, F. B.; Mead, C. A.; Truhlar, D. G.; Blais, N. C. *J. Chem. Phys.* **1987**, *86*, 6258.

(28) Bauschlicher, C. W.; Langhoff, S. R.; Partridge, H. *Chem. Phys. Lett.* **1990**, *170*, 345.

(29) (a) Schwenke, D. W.; Haug, K.; Truhlar, D. G.; Sun, Y.; Zhang, J. Z. H.; Kouri, D. J. *J. Phys. Chem.* **1987**, *91*, 6080. (b) Schwenke, D. W.; Haug, K.; Zhao, M.; Truhlar, D. G.; Sun, Y.; Zhang, J. Z. H.; Kouri, D. J. *J. Phys. Chem.* **1988**, *92*, 3202. (c) Schwenke, D. W.; Mladenovic, M.; Zhao, M.; Truhlar, D. G; Sun, Y.; Kouri, D. J. In *Supercomputer Algorithms for Reactivity, Dynamics and Kinetics of Small Molecules*; Laganà, A., Ed.; Kluwer: Dordrecht, 1989; p 131. (d) Sun, Y.; Yu, C.-h.; Kouri, D. J.; Schwenke, D. W.; Halvick, P.; Mladenovic, M.; Truhlar, D. G. *J. Chem. Phys.* **1989**, *91*, 1643.

(30) Chatfield, D. C.; Truhlar, D. G.; Schwenke, D. W. *J. Chem. Phys.*, in press.

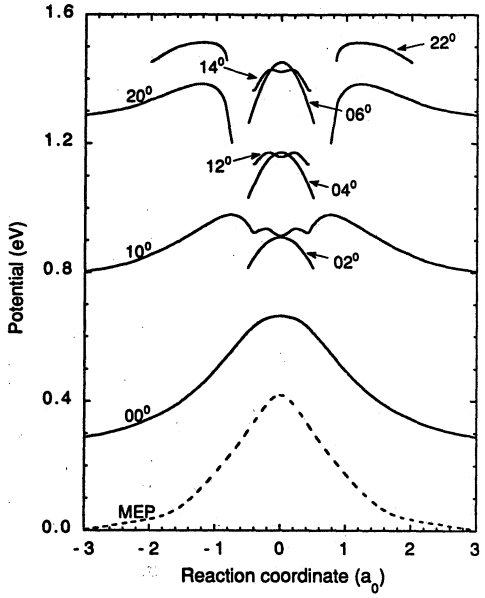

Figure 3. Vibrationally adiabatic curves for $J = 0$. The full curves are shown for $v_1 = 0$ and 1, $v_2 = 0$, and the regions near the maxima are shown for $v_1 = 0$ and 1, $v_2 \neq 0$, and $v_1 = 2$, $v_2 = 0$ and 2. $V_{MEP}(s)$ is also shown as a dashed curve.

action probability to pass from reactants to the product arrangement under consideration.[31] In a classical world the actual reactive flux[1a] is bounded from above by the generalized transition-state theory flux (this is the basis of variational transition-state theory). Thus, in a semiclassical limit we should have nine or more transition states to get $N^J_{\alpha\alpha'}(E) = 9$. In fact (see below), we believe there are actually 10 states contributing significantly to Figure 2.

To help assign the features observed in the density function, we semiclassically computed vibrationally adiabatic potential energy curves[5,6,8a-e,9,32,33] for the H + H_2 reaction using the DMBE potential energy surface. These potential curves are defined by

$$V_a^G(v_1,v_2,J,s) = V_{MEP}(s) + \epsilon_{int}(v_1,v_2,J,s) \quad (5)$$

where s is the distance along the reaction path (with $s = 0$ at the saddle point), V_{MEP} is the Born–Oppenheimer potential energy along the reaction path, and ϵ_{int} is the vibrational-rotational energy of the stretch, bend, and rotational modes excluding motion along the reaction coordinate. The reaction path is calculated as the steepest descent path in mass-scaled coordinates[33] scaled to a mass of $\mu = 2m_H/3$, where m_H is the mass of a hydrogen atom. The symmetric stretching motion of the H_3 linear saddle point correlates adiabatically with the vibrational motion in the reactant H_2 molecule. The frequencies for the stretching mode transverse to the reaction path were computed by using the WKB method,[32] and the doubly degenerate bending frequencies were obtained from a quadratic-quartic fit[16] to the bending potential. The adiabatic potential energies for $J = 0$ and various v_1, v_2 are shown in Figure 3. The adiabatic potential curves have barriers that we interpret as responsible for thresholds and wells that could support trapped states, both of which could lead to features in $\rho^J_{\alpha\alpha'}(E)$. The thresholds, which we will label $[v_1v_2^K]$, correspond to maxima in the adiabatic curves.[34] Trapped states of the linear triatomic are labeled $(v_1v_2^Kv_3)$. The semiclassically calculated values of the threshold energies are included in Table I.

To help identify those structures in the CRP plot that are due to thresholds in the adiabatic potential curves and to see if in fact all the peaks and shoulders in the density function in Figure 2

Table I. Quantized Transition States

feature	E_{max}, eV	assignment	semiclassical energy, eV	fit[a] V_β, eV	fit[a] N_B	fit[a] W_β, 10^{-2} eV
1	0.645[b]	00^0	0.663	0.645	1.01	2.02
				0.645	1.00	2.01
2	0.871	02^0	0.909	0.873	0.98	2.98
				0.873	0.98	2.97
3	0.978	10^0	0.979	0.979	0.82	0.77
				0.979	0.81	0.76
4	1.093	04^0	1.173	1.081	0.70	2.43
				1.089	0.87	2.85
5	1.186	12^0	1.173	1.186	1.27	2.52
				1.187	1.00	2.06
6	sh[c]	06^0	1.452	1.282	0.17	1.46
				1.270	0.30	2.15
7	1.369	20^0	1.384	1.368	1.02	0.79
				1.368	1.00	0.78
8	sh	14^0	1.430	1.394	0.42	1.40
				1.394	0.42	1.36
9	sh	08^0	1.754	1.454	1.01	2.84
				1.453	1.00	2.80
10	1.535	22^0	1.513	1.536	(1.51)[d]	1.58
				1.536	(1.52)[d]	1.59

[a] The first line of entries for each feature resulted from the initial least-squares fit of the density of reactive states. The second line of entries resulted from a subsequent fit with N_β for features 1, 5, 7, and 9 fixed at 1.00. [b] E_{max} is the energy of the local maximum of the density. [c] sh denotes shoulder. [d] Includes contributions from higher energy quantized transition states as discussed in Section 3.

can be explained by threshold contributions without the need to invoke trapped states, we fit the density curve to a sum of line shapes appropriate to tunneling through parabolic potential energy barriers. Note that this does not represent a claim that the true barriers are parabolic but rather represents the use of the simplest possible barrier shape for understanding the spectrum, similar to the use of a harmonic oscillator model to assign bound states.[35]

For single-channel scattering with reduced mass μ by a one-dimensional parabolic potential barrier of the form

$$V = V_{max} - \tfrac{1}{2}k(s - s_0)^2 \quad (6)$$

where $-k$ is the negative force constant, the transmission probability $P(E)$ has the form[36]

$$P(E) = [1 + \exp\{(V_{max} - E)/W\}]^{-1} \quad (7)$$

where V_{max} is the energy of the potential maximum and

$$W = (\hbar/2\pi)\sqrt{k/\mu} \quad (8)$$

To represent the density of reactive states at a threshold, $P(E)$ was differentiated with respect to energy, and a parameter N_β was introduced as a measure of the reactive flux passing through a particular quantized transition state, with index β. We denote the resulting function $\rho_\beta(E)$:

$$\rho_\beta(E) = N_\beta \frac{\exp\{(V_\beta - E)/W_\beta\}}{W_\beta[1 + \exp\{(V_\beta - E)/W_\beta\}]^2} \quad (9)$$

We then fit the solid curve of Figure 2 by a sum:

$$\rho^J_{\alpha\alpha'}(E) = \sum_\beta \rho_\beta(E) \quad (10)$$

All the features in the density curve are fit quite well with 10 terms included in the sum. The parameters from the least-squares fit are reported in Table I.

In the first fit, five of the N_β values turned out to be larger than 1, although only two are significantly larger than 1. As mentioned above, values greater than 1 are not consistent with the concept of quantized dynamical bottlenecks; these values probably result

(31) The analogy between a unit contribution to $N^J_{\alpha\alpha'}(E)$ and a single quantum state of a generalized transition state follows from the derivations of transition-state theory in refs 1d, 5a, 6, 8b, 8e, 10, and 11.
(32) Garrett, B. C.; Truhlar, D. G. *J. Chem. Phys.* **1984**, *81*, 309.
(33) Truhlar, D. G.; Kuppermann, A. *J. Am. Chem. Soc.* **1971**, *93*, 1840.
(34) When we wish to refer to an unresolved set of states differing only in K, we concatenate the superscripts, e.g., $[04^{0,2}]$ refers to $[04^0]$ and $[04^2]$.

(35) For an example of how parabolic barriers may indeed represent the multidimensional dynamics in an effective way, though, see: Skodje, R. T.; Truhlar, D. G. *J. Chem. Phys.* **1981**, *85*, 624.
(36) Kemble, E. C. *The Fundamental Principles of Quantum Mechanics*; Dover: New York, 1958.

from our assumption that the potential energy barriers are parabolic and from the difficulty of fitting overlapping structures. In addition, we have not considered the contributions from thresholds above 1.60 eV, and as a result N_β for the final feature ($\beta = 10$) includes contributions from higher energy thresholds and should not be intepreted in detail. Therefore, in a second fit to $\rho^J_{\alpha\alpha'}(E)$, we constrained N_β to 1.00 for features 1, 5, 7, and 9 and repeated the fit. The fit is still quite good, and the new values of the parameters are also given in Table I. The resulting synthetic spectrum is shown in Figure 2. A synthetic curve for the cumulative reaction probability, obtained by integrating the second fit to the density curve, is shown as a dashed curve in Figure 1; to plotting accuracy, it is indistinguishable from the accurate quantum results up until 1.6 eV.

From the parameters V_β and W_β, we can calculate hypothetical parabolic potential energy barriers for the thresholds; these are shown in Figure 4, where they are compared to the vibrationally adiabatic barriers. Since the inversion of the density to yield effective potentials does not determine s_0, all s_0 values were set equal to zero for plotting purposes.

The excellent agreement between the quantal and synthetic density of reactive states spectra (see Figure 2) leads us to believe that the global structure of the CRP can be attributed to 10 overlapping thresholds. Previously reported[20,21] converged quantal calculations of scattering matrices for H + H_2 showed energy dependences that were attributed to trapped states. We cannot unambiguously identify these quasibound states in the $\rho^J_{\alpha\alpha'}(E)$ curves because, first, features corresponding to trapped states would often be expected to lie under or overlap significantly with the threshold peaks[38] and, second, the contributions of trapped states to the density curves would be expected to be more localized than the contributions of thresholds. To avoid misinterpretation, we explicitly point out that our present results do not mean that trapped states are unimportant but rather that they show up much more strongly in state-to-state reaction probabilities than in microcanonical rate coefficients. In this regard it is worthwhile to further elaborate on the similarities and distinctions between thresholds and trapped states. As discussed above, thresholds *are* associated with a time delay (the system traverses the transition-state region slowly at a threshold), and thus they—like trapped states—may be considered a subclass of quasibound states. If a trapped state is treated in the usual way be isolated-narrow-resonance theory, its effect is local in energy; at energies more than one resonance width above the quasibound-state energy, its effect is negligible, and it leads to no lasting effect on the CRP because all $P_{\alpha'n'\alpha n}$ return, to a good approximation, to the background values they had before the resonance. But the threshold continues to gate the flux, so the cumulative reaction probability at energy E is the sum of the fluxes through *all* lower energy (i.e., open) gates. In many cases trapped states are expected to lie just below (or above) the thresholds, and our v_1, v_2, and K assignments given below show an encouraging correspondence with the resonance assignments made by Cuccaro et al.,[20] who—unlike us—assigned all time-delay features as trapped states. The agreement in assignments for v_1, v_2, and K is especially satisfying because of the different methods employed. In particular, their assignments are based primarily on time-delay and symmetry analyses, which are quite different from the procedures used here, as described below.

The present demonstration of global control in the H + H_2 reaction leads to another observation that should be made about the O + H_2 CRP, which was not brought out in previous discussions,[9h,9i,26] namely that the plateau values after the first two transition-state thresholds are very close to 1 and 2, corresponding to quantized sums of states.[37] Thus, not only is the bend-excited transition state observable as a resolvable structure, but also transition-state theory is very accurate (i.e., the plateau values are not significantly less than the number of open quantized

(37) See Figure 1 in ref 26 and note that the figure includes an extra factor of 2 because it is summed over the two identical product OH + H arrangements.

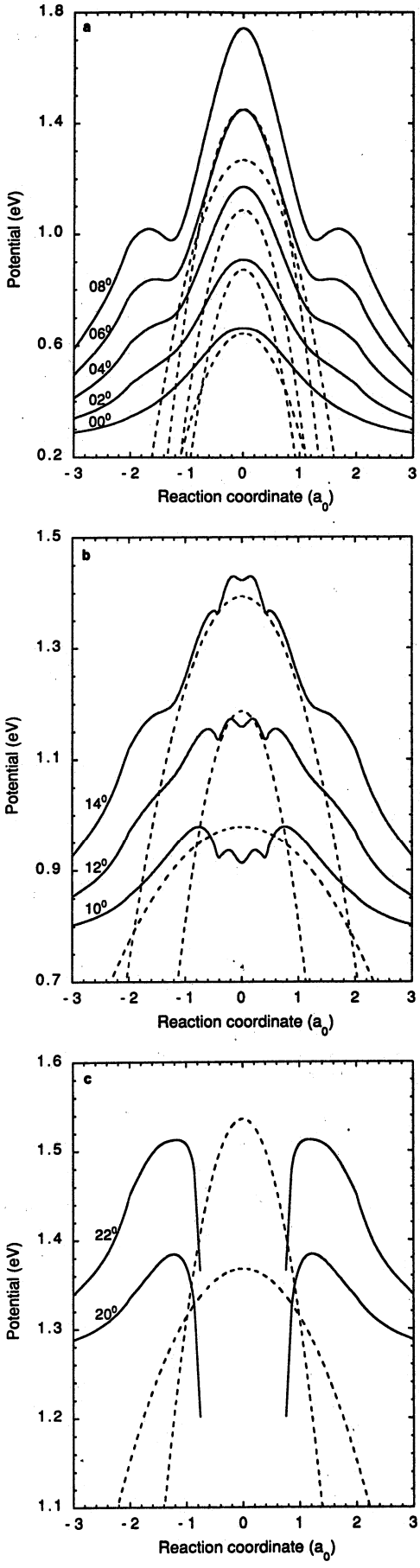

Figure 4. Vibrationally adiabatic potential curves for $J = 0$ as calculated semiclassically (solid curves) and as obtained by inverting the fits to the density of reactive states (dashed curves). (a) $v_1 = 0$, $v_2 = 0, 2, 4, 6, 8$. (b) $v_1 = 1$, $v_2 = 0, 2, 4$. (c) $v_1 = 2$, $v_2 = 0, 2$.

transition states) and the two lowest energy quantized transition states provide global control of reactivity (i.e., all the reactive flux may be associated with the rises in the CRP associated with the openings of these transition states).

To assign quantum numbers $[v_1 v_2^K]$ to the threshold features in the density of reactive states, we used a variety of methods. (i) The threshold energies V_β from the fit were compared with the semiclassical predictions in Table I. It is expected that the semiclassical threshold energies are more reliable for the low bend-excited ($v_2 = 0, 2$) quantized transition states since bending frequencies with smaller v_2 are more accurately obtained from the quadratic-quartic fit[16] to the bending potential. (ii) Energy spacings between tentatively assigned bend-excited thresholds within a stretch manifold were compared to our expectations. For example, since the $v_1 = 0$ adiabatic potential curves all have maxima at the saddle point geometry, the $v_1 = 0$ threshold energies differ only by the number of quanta in the bending mode, and therefore the threshold energy spacings should be regular. (iii) The density of reactive states was analyzed in terms of vibrationally specific densities, described below, to help assign the v_1 quantum number.

Vibrationally specific densities of cumulative reaction probability, denoted $\rho^J_{\alpha v \alpha' v'}(E)$, were obtained as analytical first derivatives with respect to energy of vibrationally specific cumulative reaction probabilities $N^J_{\alpha v \alpha' v'}(E)$. The latter quantities were obtained by selective summing as follows:

$$N^J_{\alpha v \alpha' v'}(E) = \sum_{jlj'l'} P^J_{\alpha v j l \alpha' v' j' l'}(E) \qquad (11)$$

The vibrationally specific densities shown in Figure 5 are useful because they provide an indication of the transverse stretch quantum number of the quantized transition state. Within the vibrationally adiabatic approximation, the transverse stretch quantum number v_1 identifying the vibrationally adiabatic potential curve (e.g., in Figure 3) correlates with the $v = v' = v_1$ vibrational levels of H_2 reactants and products. Thus, to the extent that there is some propensity for vibrational adiabaticity, the structure of $\rho^0_{v2v'}$ density curves for which the initial and final vibrational levels are identical is predominantly correlated with $v_1 = v = v'$ thresholds. The passage of reactive flux to products can also occur via vibrationally nonadiabatic mechanisms. These nonadiabatic transitions are reflected in the $\rho^0_{v2v'}$ density curves with $v \neq v'$; the features in these density curves might be expected therefore to show some correlation both with $[v_1 v_2^K]$ states for which $v_1 = v$ and with those for which $v_1 = v'$. Note that the finding of assignable thresholds which correlate with vibrationally adiabatic variational transition states is not inconsistent with vibrationally nonadiabatic transitions occurring between reactants and the transition state and between the transition state and products, as discussed further below.

The assignments are reported in Table I. Features 1 and 2 in Figure 2 lie at energies within 0.04 eV of the semiclassical predictions for $[00^0]$ and $[02^0]$ (see Figure 3). These threshold assignments are confirmed by analyses of the vibrationally specific density curves in Figure 5a; i.e., the fact that only ρ^0_{1020} contributes to features 1 and 2 is consistent with both corresponding to $v_1 = 0$ thresholds. Feature 1, being the overall reaction threshold, can readily be assigned as $[00^0]$. Feature 2, which corresponds to the first bend-excited threshold in the $v_1 = 0$ transverse stretch manifold, is assigned as $[02^0]$ since bending vibrations with odd quantum numbers are forbidden for $J = 0$.

Feature 3 lies within 0.001 eV of the semiclassical prediction for the $[10^0]$ threshold energy. Furthermore, in Figure 5a it can be seen that feature 3 is the first feature for which reactants in vibrational level $v = 1$ contribute significantly to the total reactive flux, as evidenced by peaks in both ρ^0_{1121} and ρ^0_{1021}. (Note that ρ^0_{1120} is identical with ρ^0_{1021} since the scattering matrix is symmetric.) Thus, both semiclassical prediction and vibrationally specific analysis support the assignment of feature 3 as $[10^0]$.

For features 4 and 5, the semiclassical results are not sufficient to make the assignments. Two thresholds, $[04^0]$ and $[12^0]$, are predicted to lie at energies in the vicinity of feature 5, while none

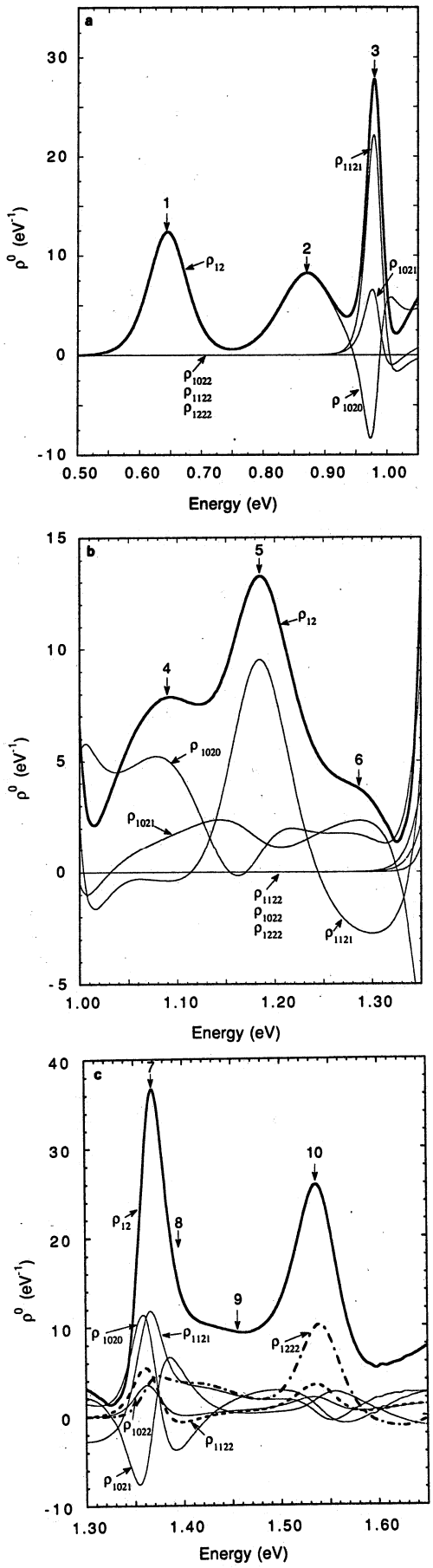

Figure 5. Vibrationally specific CRPs for $J = 0$. (a) Low energy; (b) mid energies; (c) high energy.

are predicted to lie at the energy of feature 4. However, the density functions ρ^0_{1020} and ρ^0_{1121}, shown in Figure 5b, reveal that features 4 and 5 consist predominantly of reactive flux out of $v = 0$ and 1, respectively. Therefore, feature 4 is assigned as [04^0] and feature 5 as [12^0].

Feature 6 appears as a shoulder on the peak identified above as [12^0]. The close agreement between the quantal density curve and the synthetic fit (see Figure 2) suggests that feature 6 is a threshold. From the energy spacings of the bend-excited thresholds already identified within the $v_1 = 0$ manifold ([00^0], [02^0], and [04^0]), the [06^0] state would be expected, if observable, to lie near the threshold energy of feature 6. Furthermore, we see that the vibrationally specific density curve ρ^0_{1020} peaks near feature 6, while ρ^0_{1121} exhibits a minimum and ρ^0_{1222} remains constant at zero; these observations are consistent with feature 6 being assigned to a $v_1 = 0$ threshold (see Figure 5b). On this basis, feature 6 is assigned as [06^0].

It can be seen in Figure 3 that above about 1.3 eV semiclassical calculations predict a rather high density of states due to the appearance of the $v_1 = 2$ adiabatic threshold. In particular, [20^0] and [14^0] are both predicted semiclassically to lie between 1.36 and 1.44 eV. The fit to quantal results indicates that features 7 and 8 both fall within this energy range, occurring close together under the peak near 1.37 eV. We assign feature 7 on the basis of the semiclassical adiabatic calculations. These calculations yield a [20^0] state 0.02 eV below feature 7, and since this is a ground-bend threshold, it is expected to be reasonably accurate. This assignment is supported by the fact that feature 7 is the first feature with a significant contribution from $v = 2$, as shown by peaks in ρ^0_{1022}, ρ^0_{1122}, and ρ^0_{1222} near 1.37 eV in Figure 5c. (We do not understand why the ρ^0_{1020} curve exhibits a maximum near 1.37 eV. One possibility is that there is a trapped state[38] at an energy just below the [20^0] threshold and that this has a significant effect on the densities.)

Vibrationally specific density curves as well as semiclassical adiabatic curves suggest the assignment of feature 8 as [14^0], and energy spacings within the $v_1 = 0$ stretch manifold make a [08^0] assignment unlikely. Density curve ρ^0_{1121}, which at lower energies shows positive correlation only with $v_1 = 1$ thresholds, peaks at a slightly higher energy than ρ^0_{1022} and ρ^0_{1122}. Furthermore, while ρ^0_{1021} exhibits a minimum and ρ^0_{1022} and ρ^0_{1122} exhibit maxima near feature 7, ρ^0_{1021} exhibits a maximum and ρ^0_{1022} and ρ^0_{1122} exhibit minima near feature 8. This suggests that the passage of flux from reactants in vibrational level $v = 0$ to products in other vibrational levels yields preferentially $v' = 2$ at the energy of feature 7 and preferentially $v' = 1$ at the energy of feature 8. This is consistent with the above assignment of feature 7 and the assignment of feature 8 as [14^0].

The assignment of feature 9 as [08^0] is deduced from an analysis of the spacings within the $v_1 = 0$ vibrational manifold and from the observation that the density curve ρ^0_{1020} exhibits a broad peak in the vicinity of this feature while none of the other vibrationally specific density curves show much structure. The broadness of this feature and the expectation that threshold effects diminish as the bend quantum number increases make this assignment less definitive. Although the quantal density curve in Figure 2 does not readily show a feature between the peaks at 1.37 and 1.54 eV, the threshold features 7, 8, and 10 can only account for 10% of the observed quantal density at 1.45 eV, leading us to believe that the existence of another threshold (i.e., feature 9) at this energy in the fit is indeed a physical result.

The threshold energy V_β for feature 10 differs by only 0.02 eV from the semiclassical prediction for [22^0], and the vibrationally specific density curves involving reactive flux into $v' = 2$ (ρ^0_{1222}, ρ^0_{1022}, and ρ^0_{1122}) all exhibit peaks at the energy of this feature. Thus, we assign feature 10 as [22^0].

With all of the features assigned, it is interesting to relate trends in the fitted parameters N_β and W_β to the threshold assignments. As mentioned above, if each threshold were an ideal quantized dynamical bottleneck, the value of N_β would be 1 in every case. For all the thresholds with $v_2 = 0$ or 2, this is the case to within 19%. For several of the thresholds with highly excited bends, however, the value of N_β falls significantly below 1. There are a number of possible explanations for this. For example, the N_β values result quantitatively from the assumption of a parabolic form for the effective potential energy barrier, and this idealization may lead to quantitative errors. We also note that flux through a quantized bottleneck may decrease at energies above the threshold to which it corresponds, since recrossing effects increase with energy.[1d,1e]

The parameter W_β, which is related to the force constant for the parabolic potential barrier, becomes larger as the bend quantum number is increased from 0 to 2 within each transverse stretch manifold. This is consistent with the observation that the adiabatic potential becomes narrower as v_2 increases. Narrow barriers will allow a significant amount of tunneling and hence will result in broad peaks in the density curve.

We especially emphasize that the reaction is not globally adiabatic, especially in the asymptotic j and l quantum numbers which correspond, respectively, to diatomic rotation and orbital angular momentum of relative translation and which correlate[8c,8d] at the transition states with bending motion and overall triatomic rotation and also in the stretch vibrational quantum number. However, adiabaticity is a sufficient but not necessary criterion for the validity of transition-state theory,[39] and the analysis presented here shows that the nonadiabatic flux is "focused" in the interaction region through a sequence of discrete transition states whose energies correlate well with locally adiabatic structures. That is, adiabaticity is a better approximation at the transition state or threshold itself than globally. One way to understand this is to note that at a threshold the reaction coordinate motion is effectively stopped (at least classically) and thus the simplest criterion for vibrational adiabaticity, namely that vibrational modes transverse to the reaction coordinate are fast compared to motion along the reaction coordinate, is nominally satisfied. Further work is required to make these notions more quantitative.

Spectroscopic Constants. We have seen that the global structure of the cumulative reaction probability for $J = 0$ is controlled by 10 quantized transition states, for which we can assign bend and stretch quantum numbers to the modes orthogonal to the reaction coordinate. In addition, as discussed in more detail below, the $J = 4$ cumulative reaction probability shows similar thresholds. We obtained spectroscopic constants for these quantized transition states by fitting the [00^0], [02^0], [04^0], [10^0], [12^0], and [20^0] states for $J = 0$ and the [00^0] state for $J = 4$ by[24,40]

$$E(v_1v_2)/hc = E_0/hc + \omega_1(v_1 + 0.5) + x_{11}(v_1 + 0.5)^2 + \omega_2(v_2 + 1) + x_{22}(v_2 + 1)^2 + x_{12}(v_1 + 0.5)(v_2 + 1) + BJ(J + 1) \quad (12)$$

where E_0 is a constant and ω_1, ω_2, x_{11}, x_{12}, x_{22}, and B are the usual spectroscopic fit parameters. Using the final V_β values of Table I for $J = 0$ and 0.671 eV [the position of the first peak in $\rho^4_{\alpha\alpha'}(E)$] for the [00^0] state with $J = 4$ yields the following values for the spectroscopic constants (in cm^{-1}): $\omega_1 = 2331$, $\omega_2 = 1008$, $x_{11} = 222$, $x_{22} = -12$, $x_{12} = -81$, and $B = 10.5$. The root mean square deviation of eq 12 to the nine energy differences with $J = 0$ is 0.015 eV = 121 cm^{-1}. In the units more commonly used for chemical kinetics, this is a very small deviation, i.e., 0.35 kcal/mol. Although this rms error can be reduced to 0.007 eV by a least-squares fit employing all nine energy differences, the parameters based on the low-lying levels, as given above, represent a more systematic treatment and will be used for further analysis.

The value of 10.5 cm^{-1} calculated for the rotational constant B from the present analysis of quantized transition states observed

(38) For example, our vibrationally adiabatic calculations predict a trapped state 0.023 eV below [10^0] and another 0.049 eV below [20^0].

(39) See refs 1d, 5a, 8a, 8e, and: (a) Marcus, R. A. *J. Chem. Phys.* **1968**, *49*, 2617. (b) Quack, M.; Troe, J. *Gas Kinet. Energy Transfer* **1977**, *2*, 175. (c) Truhlar, D. G. *J. Phys. Chem.* **1979**, *83*, 188. (d) Marcus, R. A. *J. Phys. Chem.* **1979**, *83*, 204.

(40) Califano, S. *Vibrational States*; Wiley: London, 1976; p 271.

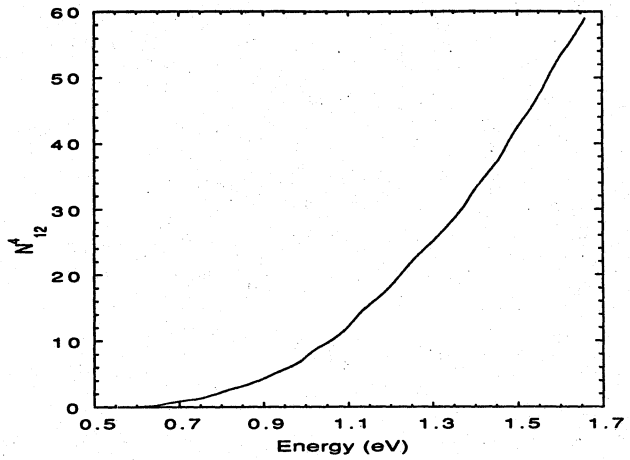

Figure 6. Cumulative reaction probability for $J = 4$. The curve is a spline fit to the accurate quantal results.

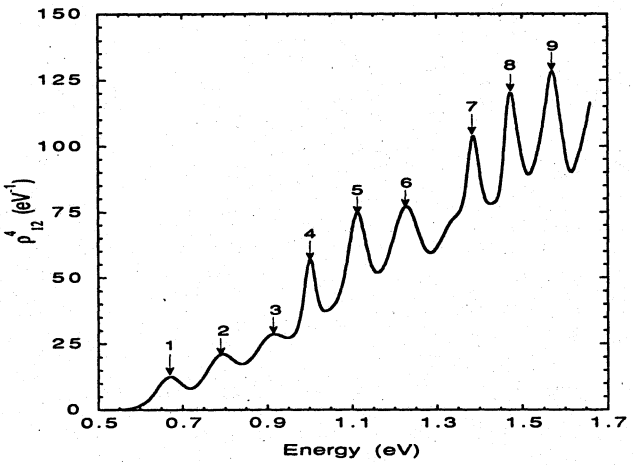

Figure 7. Accurate quantal density of reactive states for $J = 4$ obtained by differentiation of the curve in Figure 6. The feature numbers correspond to the local maxima of the density.

in the microcanonical rate constants is similar to values obtained from some previous analyses of transition states and resonances. For example, the conventional transition state (saddle point) for this potential energy surface has nearest-neighbor distances of 1.755 a_0,[5h] from which the moment of inertia $I^\ddagger$ is 1.13×10^4 atomic units, and $B^\ddagger_e \equiv (2I^\ddagger)^{-1} = 9.7$ cm^{-1}. The variational transition-state value for [00^0] would be the same since the variational transition state is at the saddle point in this case.[5h] Bowman[7a] used a value of 10.3 cm^{-1} for the energy-shift approximation to the CRP on an older, less accurate potential energy surface,[41] for which we calculate from the moment of inertia that $B^\ddagger_e$ also equals 10.3 cm^{-1}. Pollak,[42] using a more accurate potential energy surface,[43] a stability analysis of resonant periodic orbits, and a semiclassical adiabatic reduction method,[44] calculated $B = 7.8$ cm^{-1} for the lowest energy trapped state. In our own previous work, we obtained the value of 9 cm^{-1} for the ($1v_2^K0$) quasibound state manifold observed in state-to-state quantal transition probabilities,[21] and we obtained values from 8.0 to 9.2 cm^{-1} for various quasibound states by earlier semiclassical calculations.[19b]

$J = 4$. Plots of $N^4_{\alpha\alpha'}(E)$ and $\rho^4_{\alpha\alpha'}(E)$ are given in Figures 6 and 7. The density of states for $J = 4$ is considerably greater than that for $J = 0$ since odd bend quantum numbers are allowed for $J = 4$ but not for $J = 0$ and since the degeneracy of excited bend states increases until $v_2 = J$. This is reflected in $N^4_{\alpha\alpha'}(E)$, for which the steplike structure is not as evident as for $N^0_{\alpha\alpha'}(E)$, and in $\rho^4_{\alpha\alpha'}(E)$, which does not approach as close to zero as $\rho^0_{\alpha\alpha'}(E)$ does between peaks since features overlap more.

Table II. Quantized Transition States for $J = 4$

feature	E_{max}, eV	$N^4_{\alpha\alpha'}$	state	$E^{(1)}(v_1v_2)$, eV	$V^A_a(v_1v_2)$, eV	$N^{QTST}_{\alpha\alpha'}$
1	0.671	1	00^0	0.671	0.687	1
2	0.794	3	01^1	0.783	0.810	3
3	0.917	$5^1/_2$	$02^{0,2}$	0.899	0.939	6
4	1.002	$9^1/_2$	10^0	1.005	0.997	
			$03^{1,3}$	1.009	1.073	11
5	1.113	16	11^1	1.111	1.083	
			$04^{0,2,4}$	1.115	1.212	18
6	1.228	24	$12^{0,2}$	1.213	1.202	
			$05^{1,3}$	1.219	1.356	25

Clearly not all quantized transition states lead to easily distinguished features for this case with a higher density of states, but we can relate the structure to that for $J = 0$. To do this, we have numbered the prominent peaks in the density for discussion purposes. It was possible to assign several of the peaks simply by comparing the energies of the quantal density peak maxima with semiclassical predictions and with spectroscopic energies predicted by eq 12. These assignments are given strong support by the increments of the cumulative reaction probability corresponding to each peak, which can be compared with the values that would be expected for a given assignment if generalized transition-state theory were exact with unit transmission coefficients, i.e., as if all N_β were unity.

These assignments are reported in Table II. In this table E_{max} is the energy of the peak in $\rho^4_{\alpha\alpha'}(E)$; $N^4_{\alpha\alpha'}$ is the value of the $J = 4$ cumulative reaction probability at the first local minimum following the peak; $E^{(1)}(v_1v_2)$ is the energy computed for a given state by eq 12, i.e., including anharmonicity through first order; $V^A_a(v_1v_2)$ is the maximum of the semiclassical vibrationally adiabatic curve for this v_1 and v_2; and $N^{QTST}_{\alpha\alpha'}$ is the sum of the degeneracies for a state and all states listed above it.

Features 1, 2, and 3 can be assigned on the basis of semiclassical threshold energies as [00^0], [01^1], and [02^{0,2}], respectively. (We do not consider the splitting of quantized transition states having the same v_1 and v_2 quantum numbers but differing in vibrational angular momentum K.) As can be seen in Table II, the rise in $N^4_{\alpha\alpha'}(E)$ associated with each of these peaks is very close to that expected for these assignments, i.e., 1, 2, and $2^1/_2$ vs the degeneracies of 1, 2, and 3 for the states [00^0], [01^1], and [02^{0,2}], respectively. The energy shifts between the $J = 0$ and $J = 4$ features with the same v_1, v_2 are somewhat less consistent on a relative scale, 0.026 eV for [00^0] and 0.044 eV for [02^{0,2}], but the 0.018-eV difference between these numbers is acceptably small on an absolute scale and can be accounted for entirely in terms of nonideality of the [02^{0,2}] peak shape and the neglected splitting of [02^0] from [02^2].

Feature 4 occurs very close (within 0.005 eV) to the semiclassical prediction for [10^0]. From the spectroscopic parameters, it is predicted that not only [10^0] but also [03^{1,3}] will occur near feature 4. This is consistent with the value of the cumulative reaction probability, which is shown in Table II to be $9^1/_2$ after feature 4. A value of 11 would be predicted if each of the thresholds so far assigned, including both [10^0] and [03^{1,3}], were present with its full degeneracy and gated reactive flux with unit transmission coefficient.

From the spectroscopic parameters, [11^1] and [04^{0,2,4}] are predicted near feature 5, and [12^{0,2}] and [05^{1,3}] are predicted near feature 6. Furthermore, the semiclassical threshold energies for [11^1] and [12^{0,2}] are within 0.03 eV of the E_{max} values for features 5 and 6. It is not surprising that the semiclassical predictions for [04^{0,2,4}] and [05^{1,3}] appear to be too high; this was often the case for highly bend excited states for $J = 0$. Thus, features 5 and 6, like feature 4, each appear to result from the cumulative effect of two quantized transition states. The accurate values of $N^4_{\alpha\alpha'}(E)$ are in excellent agreement with the values predicted on the basis

(41) Porter, R. N.; Karplus, M. *J. Chem. Phys.* **1964**, *40*, 1105.
(42) Pollak, E. *J. Phys. Chem.* **1986**, *90*, 3619.
(43) (a) Liu, B. *J. Chem. Phys.* **1973**, *58*, 1925. (b) Siegbahn, P.; Liu, B. *J. Chem. Phys.* **1978**, *68*, 2457. (c) Truhlar, D. G.; Horowitz, C. J. *J. Chem. Phys.* **1979**, *68*, 2466.
(44) Pollak, E.; Wyatt, R. E. *J. Chem. Phys.* **1984**, *81*, 1801.

of these assignments, i.e., 16 after peak 5 and 24 after peak 6 compared with predicted values of 18 and 25.

A large number of states are expected at energies between 1.28 eV, corresponding to the local minimum between features 6 and 7, and 1.61 eV, corresponding to the local minimum after feature 9, namely the $v_2 = 6$–9 states of the $v_1 = 0$ manifold, the $v_2 = 3$–6 states of the $v_1 = 1$ manifold, and the $v_2 = 0$–2 states with $v_1 = 2$. Although we do not make detailed assignments in this region, we note from comparisons with $J = 0$ that thresholds $[20^0]$, $[21^1]$, and $[22^{0,2}]$ probably contribute to peaks 7, 8, and 9, respectively. Even without assigning the remaining states listed above to particular features in the density plot, the value of the accurate cumulative reaction probability can be seen to be in good agreement with quantized transition-state theory. In particular, the accurate cumulative reaction probability at 1.61 eV is $54^1/_2$, which compares with the predicted value of 67 obtained by adding the sum of the degeneracies of these states to 25. Thus, quantized transition-state theory appears to be about 23% high, which is a bit larger than the overestimate for $J = 0$ at 1.6 eV.

Our success in correlating the features of the density curves with quantized transition states for both $J = 0$ and $J = 4$ demonstrates that $H + H_2$ chemical reactivity is globally controlled by quantized transition states associated with maxima of vibrationally adiabatic potential curves. It has previously been recognized that quantized transition states play a dominant role in chemical reactivity at low energies, for example,[2,5,7,9,12] at energies in the vicinity of the overall reaction threshold which controls thermal rate constants and in one case—the analysis in ref 26 of the accurate quantum dynamical calculations of refs 9h and 9i—at a bend-excited threshold. Here we show that the global control of reactivity by transition states persists up to at least 1 eV beyond the first threshold. Thus, we find strong evidence for transition states which can be thought of as quantized dynamical bottlenecks controlling the passage of reactive flux to products.

$J = 1$. Results for $J = 1$ are consistent with those presented above, and so we do not present the analysis in detail.

4. Summary and Concluding Remarks

The energy dependence of the cumulative reaction probability for the $H + H_2$ reaction between 0.3 and 1.6 eV is globally controlled by a series of 10 thresholds for $J = 0$ at energies up to 1.6 eV and by 9 thresholds for $J = 4$ at energies up to 1.28 eV. These thresholds dominate the dynamics of the reaction for the entire range of energies relevant to thermal rate constants. The CRP structures are enhanced by calculating the derivative of the cumulative reaction probability with respect to energy. The derivative analyses for $J = 0$ and 1 show features at similar energies to the metastable states identified by Cuccaro et al.[20] with collision lifetime analysis. A comparison of the present quantal results to semiclassical results obtained by using variational transition-state theory leads us to interpret the structures in the CRPs as being predominantly due to thresholds rather than trapped states. The thresholds are manifestations of quantized dynamical bottlenecks through which the flux is channeled from reactants to products. We have been able to assign stretch and bend quantum numbers to these quantized transition states by utilizing semiclassical adiabatic potentials and vibrationally specific cumulative reaction probabilities. Also, we have successfully reproduced the features in the density curves by employing a simple model of semiclassical scattering off of parabolic potential energy barriers. We often find that the quantized transition states allow flux to pass from reactants to products with unit efficiency. This provides strong support for the assumptions of quantized variational transition-state theory[5,6,9,16] even at energies quite high above the overall threshold. It also supports the use of quantized transition states in other calculations employing conventional or generalized transition states.[7,8,11,17,18,26,45,46]

A critical strength of our analysis is that quantum mechanical analogues of classical phase space bottlenecks are identified by a phenomenological analysis of an observable quantity, namely the cumulative reaction probability, which—within a factor proportional to the nondynamical reactant density of states—is just the microcanonical reaction rate constant. In addition, we find that the observed quantized transition states correlate well in their energies and degeneracies, and to some extent their widths, with a model based on adiabatic variational transition states. A weak point of that analysis is the treatment of anharmonicity in the model calculations, especially the effect of mode–mode coupling on the bending excitations.

A common paradigm of chemical reaction dynamics for simple barrier reactions is that most reactive flux is direct or nonresonant, and this direct reaction reactive flux is accompanied at certain energies by resonant contributions mediated by metastable states with assignable quantum numbers.[19–21,47] (In this view, the resonant states lead to "special features" or "anomalies".[48]) In a refined version of this picture we also recognize that the threshold for direct scattering may be associated with a vibrationally adiabatic threshold with transition-state quantum numbers, i.e., quantum numbers for all degrees of freedom except a reaction coordinate, in which the energy is continuous. In the present paper we have shown that, at least for one simple reaction, *all* reactive flux may be associated with passage through a sequence of resolvable quantized transition states with assignable quantum numbers. This analysis brings out the quantum structure of the entire reactive process rather than just the resonant part superimposed on an unassigned background.

The quantized transition states may be considered as an extension of the successful application of vibrationally adiabatic models to higher energies, or—in a more general sense—as evidence for the dominance of reactivity by quantum mechanical analogues of the recently heavily studied classical phase space structures that may be shown to limit or gate the flux from one region of phase space to another. Further connections along the latter direction would be very interesting. We simply note here that identifying such structures in model systems and then quantizing them and predicting their consequences in real systems has proved very challenging, but the present approach has found the role of quantized transition states by a more direct route—namely phenomenological analysis of accurate quantum microcanonical rate constants for a simple, but real, chemical reaction.

The new technique that we have employed to discover the underlying quantum number structure of the reactive flux is to plot the energy derivative of the accurate quantal cumulative reaction probability. This quantity, called the density of reactive states, is the accurate quantal analogue of the variational transition-state theory density of states of the generalized transition state. This analysis allowed us to bring out the discrete structure of the dynamical bottlenecks.

5. Acknowledgments

We are grateful to Gillian Lynch for help with the calculations and to Donald J. Kouri for helpful discussions. Our work on accurate quantum dynamics is supported in part by the National Science Foundation and NASA, and our work on variational transition state theory is supported in part by the U.S. Department of Energy, Office of Basic Energy Sciences.

(45) Bowman, J. M.; Lee, K.-T.; Ju, G.-Z. *Chem. Phys. Lett.* **1982**, *86*, 384. Sun, Y.; Bowman, J. M.; Schatz, G. C.; Sharp, A. R.; Connor, J. N. L. *J. Chem. Phys.* **1990**, *92*, 1677.

(46) The literature dates back to the 1930s (ref 17), and the references given are representative, not exhaustive.

(47) See also, e.g.: Feshbach, H. *Ann. Phys. (N.Y.)* **1962**, *19*, 287.

(48) Levine, R. D.; Bernstein, R. B. *Molecular Reaction Dynamics and Chemical Reactivity*; Oxford University Press: New York, 1987; pp 409–410.